Received: 15 April 2021 | Revised: 30 July 2021 | Accepted: 23 August 2021

DOI: 10.1111/ejn.15442

RESEARCH REPORT

EJN European Journal of Neuroscience FENS WILEY

Optogenetic stimulation of VIPergic SCN neurons induces photoperiodic-like changes in the mammalian circadian clock

Michael C. Tackenberg[1,2] | **Jacob J. Hughey**[1,2] | **Douglas G. McMahon**[1,3]

[1]Department of Biological Sciences, Vanderbilt University, Nashville, TN, USA

[2]Department of Biomedical Informatics, Vanderbilt University Medical Center, Nashville, TN, USA

[3]Vanderbilt Brain Institute, Vanderbilt University, Nashville, TN, USA

Correspondence
Douglas G. McMahon, Vanderbilt Brain Institute, Vanderbilt University, Nashville, TN, USA.
Email: douglas.g.mcmahon@vanderbilt.edu

Funding information
NIH, Grant/Award Numbers: R01 GM117650, R35 GM124685

Edited by: Antoine Adamantidis

Abstract

Circadian clocks play key roles in how organisms respond to and even anticipate seasonal change in day length, or photoperiod. In mammals, photoperiod is encoded by the central circadian pacemaker in the brain, the suprachiasmatic nucleus (SCN). The subpopulation of SCN neurons that secrete the neuropeptide VIP mediates the transmission of light information within the SCN neural network, suggesting a role for these neurons in circadian plasticity in response to light information that has yet to be directly tested. Here, we used in vivo optogenetic stimulation of VIPergic SCN neurons followed by ex vivo PERIOD 2::LUCIFERASE (PER2::LUC) bioluminescent imaging to test whether activation of this SCN neuron subpopulation can induce SCN network changes that are hallmarks of photoperiodic encoding. We found that optogenetic stimulation designed to mimic a long photoperiod indeed altered subsequent SCN entrained phase, increased the phase dispersal of PER2 rhythms within the SCN network, and shortened SCN free-running period—similar to the effects of a true extension of photoperiod. Optogenetic stimulation also induced analogous changes on related aspects of locomotor behaviour in vivo. Thus, selective activation of VIPergic SCN neurons induces photoperiodic network plasticity in the SCN that underpins photoperiodic entrainment of behaviour.

KEYWORDS
biological rhythms, circadian, photoperiodism, rhythms, suprachiasmatic nucleus

Abbreviations: ANOVA, analysis of variance; CCD, charge-coupled device; ChR2, channelrhodopsin-2; DD, dark/dark (constant darkness); DMEM, Dulbecco's modified Eagle medium; GABA, gamma-aminobutyric acid; HBSS, Hank's balanced salt solution; HEPES, 4-(2-hydroxyethyl)-1-piperazineethanesulfonic acid; ICCD, intensified charge-coupled device; IQR, interquartile range; LD, light/dark; LED, light emitting diode; LSP, Lomb–Scargle periodogram; PCR, polymerase chain reaction; PER2, Period 2; PER2::LUC, Period 2::Luciferase; PID, passive infrared detection; PVN, pariventricular nucleus; ROI, region of interest; SCN, suprachiasmatic nucleus; SPZ, subparaventricular zone; VIP, vasoactive intestinal polypeptide; ZT, Zeitgeber time.

1 | INTRODUCTION

In mammals, circadian responses to seasonal changes in photoperiod are encoded by the master clock, the suprachiasmatic nucleus (SCN) of the hypothalamus (Tackenberg & McMahon, 2018). How the SCN network initiates and maintains its response to changing photoperiod is not fully understood, but several lines of evidence

point to a role for the subpopulation of SCN neurons that express vasoactive intestinal polypeptide (VIP). VIPergic neurons relay photic information from the retina, even when their individual cellular clocks are deficient (Shan et al., 2020), and their activity is required for clock resetting from light exposure (Jones et al., 2018). VIP itself is necessary for the induction of locomotor behaviour duration after-effects (Lucassen et al., 2012). Considering that long photoperiods extend the high-firing phase of the daily electrical rhythm of the SCN (VanderLeest et al., 2007), we hypothesized that direct activation of VIP neurons may induce photoperiodic encoding. Here we tested that hypothesis by optogenetically stimulating VIPergic SCN neurons in vivo during the hours following lights off to effectively extend the daily photoperiod duration in mice entrained to a short photoperiod. We then measured effects on the SCN network in ex vivo assays.

We bred mice expressing both the PERIOD 2::LUCIFERASE (PER2::LUC) reporter and VIP-driven channelrhodopsin (VIP-ChR2), as well as non-ChR2 PER2::LUC control mice (ChR2-Neg), then implanted each mouse with a fibre optic targeting the SCN. We exposed mice to 8 h of light, 8 h of fibre optic stimulation in the dark, and 8 h of unstimulated dark each day for 7 days. We then extracted and cultured 300-μm SCN slices and measured PER2::LUC expression rhythms for 6 days using an ICCD camera.

Using the peak times of the PER2::LUC rhythm for each of several thousand ~10 × 10 μm regions-of-interest (ROIs) from each SCN, we constructed a relative phase map of the SCN clock network for each slice at each daily rhythmic peak (Figures 1a and S1-2). These maps indicated that phase variation increased in both groups over time (an effect also seen in the overall frequency

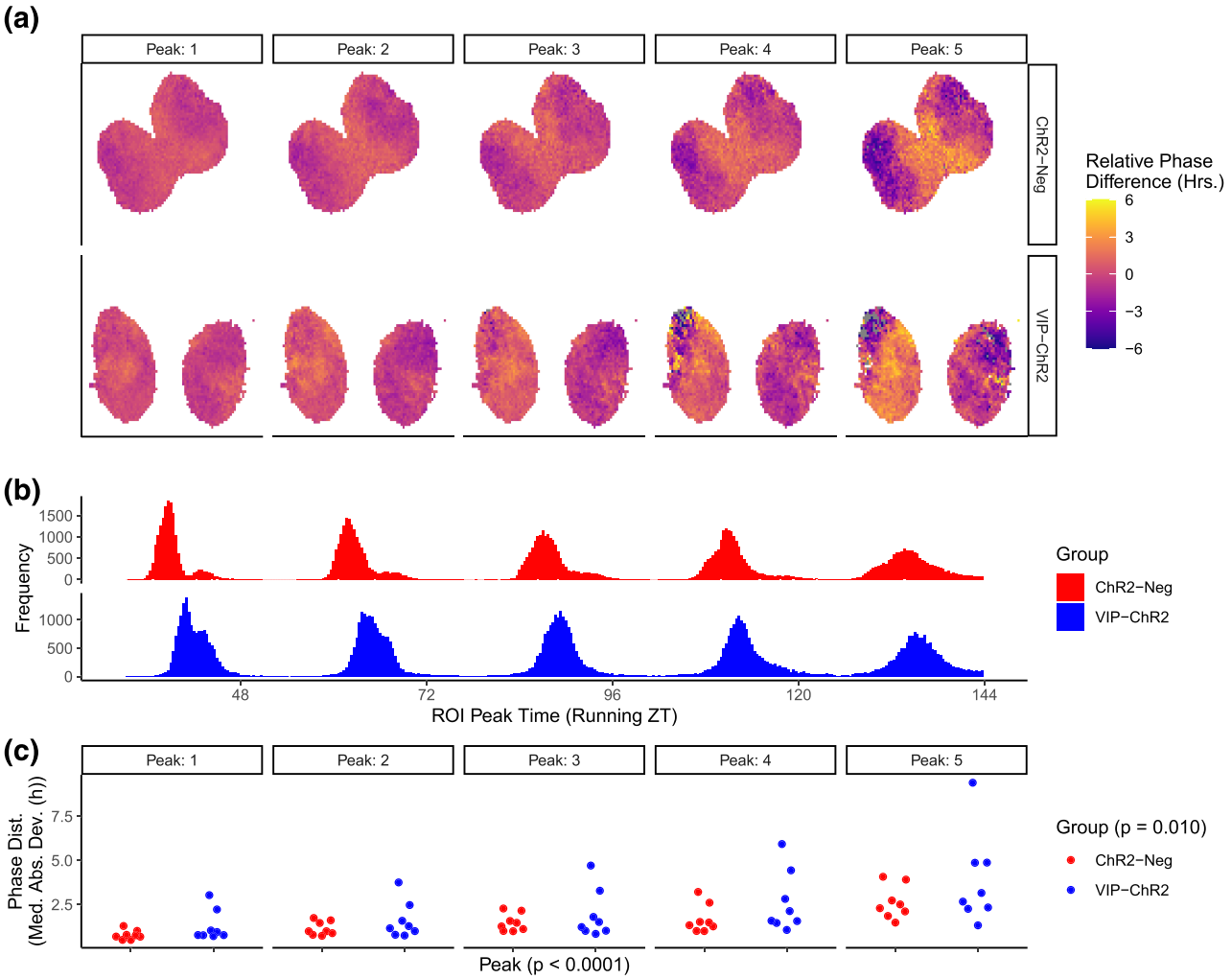

FIGURE 1 Optogenetic stimulation of VIPergic neurons influences SCN circadian phase distribution. (a) Representative heat maps showing the relative phase of the PER2::LUC rhythm for each ROI, for each peak (see also Figure S2). (b) Frequency distribution of the ROI peak time of each group (see also Figure S1). (c) the median absolute deviation of the peak time for each peak in each slice. Peak and group *p* values indicated are the main effects of an ordinary two-way ANOVA

distributions of peak timing for each group shown in Figure 1b) and that medial regions of the SCN became phase advanced relative to lateral regions. To quantify the phase variation for each group over time, we calculated the median absolute deviation in ROI phase for each slice in each cycle (Figure 1c). In contrast to previous studies using 16:8 LD (Buijink et al., 2016; Tackenberg et al., 2020) or 20:4 LD (Evans et al., 2013), the median absolute deviation of peak time for the first cycle was not significantly different between groups ($p = 0.09$). Based on all five cycles, however, the phase distribution was significantly wider for VIP-ChR2 slices than for control slices ($p = 0.010$, two-way ANOVA main effect of group), with a significant increase over time for both groups combined ($p < 0.0001$, two-way ANOVA main effect of peak) and no significant interaction ($p = 0.306$, two-way ANOVA interaction effect). The significant main effect of group in the absence of a significant interaction effect of group over time indicates that changes in network stability affect both groups similarly. The broadened SCN phase distribution in response to VIPergic SCN neuron activation is therefore in line with previously observed phase distribution following exposure to a 16:8 long photoperiod compared with 8:16 short (Buijink et al., 2016; Tackenberg et al., 2020).

To determine if an unintentional offset of optogenetic fibre placement resulted in bias in our measurement through the induction of more asymmetric stimulation of the SCN in one group compared with the other, we used *k*-means clustering to sort the ROIs based on their XY position, which successfully discriminated between each half of the SCN (Figure S3A,B). We then measured the left–right difference in median absolute deviation of each SCN (Figure S3C), revealing no significant effect of group on any left–right median absolute deviation difference ($p = 0.697$, two-way ANOVA, main effect of group).

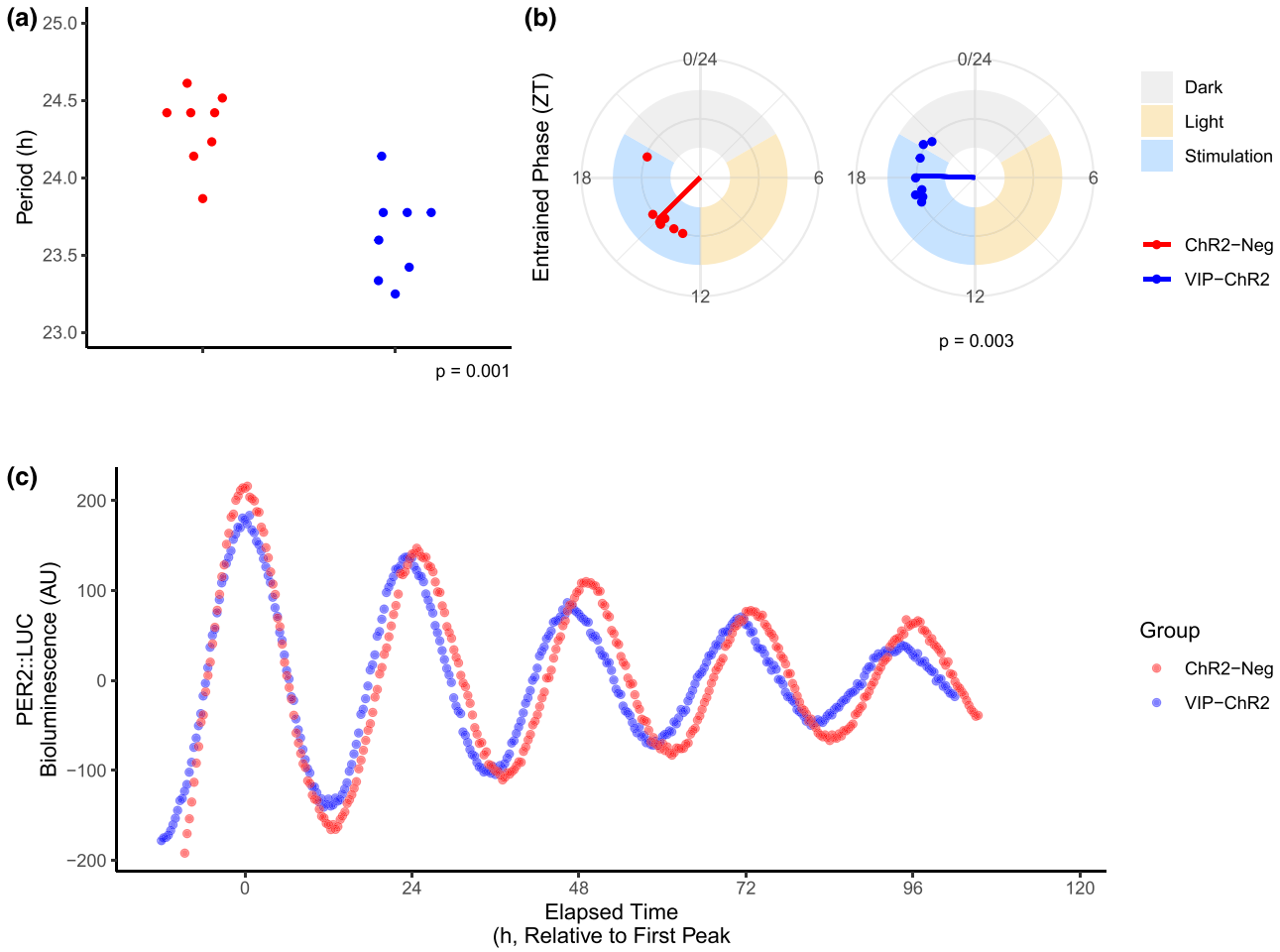

FIGURE 2 Optogenetic stimulation of VIPergic neurons influences SCN free-running period and entrained phase. (a) Free-running period of the PER2::LUC rhythm as measured by LSP on ~6 cycles of luminescence. The indicated *p* value is the result of a Kruskal–Wallis test. (b) Circular plots showing the first peak time of each slice in ZT. The indicated *p* value is the result of a circular ANOVA. Shaded regions represent the lighting conditions of the previous cycle at that phase. (c) Representative baseline-subtracted PER2::LUC bioluminescence traces from ChR2-neg (red) and VIP-ChR2 (blue) slices

We next measured the free-running period of the overall PER2::LUC rhythm in the SCN slices from each group using the Lomb–Scargle periodogram (LSP, Figure 2a; Tackenberg & Hughey, 2021). PER2::LUC free-running period was significantly shorter ($p = 0.001$, Kruskal–Wallis test) in slices from VIP-ChR2 mice (median period 23.68, IQR 0.38 h) than in slices from ChR2-Neg mice (median period 24.42, IQR 0.23 h). The effect of VIPergic SCN neuron stimulation therefore mimics the effect of long photoperiod exposure ex vivo (Ciarleglio et al., 2011; Myung et al., 2015).

To determine the phase angle of entrainment (the relative alignment of the SCN PER2::LUC rhythm with the previous entraining LD cycle), we determined the mean peak time of the first peak relative to the last lights-off transition before slicing (Figure 2b). The mean phase of the first peak in VIP-ChR2 slices (ZT 18.12, circular SD 0.42 h) was significantly delayed ($p = 0.003$, circular ANOVA) compared with that of the ChR2-Neg slices (ZT 15.02, circular SD 0.45 h), reflecting the phase delay induced by the repeated daily extended stimulation.

We performed a parallel experiment to determine if the plasticity we observed in the SCN ex vivo in response to targeted stimulation of VIPergic neurons was also observable in behavioural changes in vivo. We measured locomotor activity of VIP-ChR2 and ChR2-Neg mice via passive infrared detection (PID). We exposed the mice to 5 days of short photoperiod (8:16 light:dark, h) followed by 7 days of 8 h light, 8 h stimulation in the dark, and 8 h of unstimulated darkness. We then untethered the mice and transferred the cages into constant darkness (DD) for 7 days (Figures 3a and S6).

Using the LSP on the DD portion of the activity record for each mouse, we found free-running period was significantly shorter in VIP-ChR2 mice (median 22.71, IQR 0.36 h) than in ChR2-Neg mice (median 23.72, IQR 0.25 h; $p = 0.013$, Kruskal–Wallis test; Figure 3b). This difference in period is similar to that reported for period after-effects induced by long and short photoperiods (Pittendrigh & Daan, 1976; Tackenberg et al., 2020) and similar to the difference we observed ex vivo (Figure 2a), indicating that extended stimulation of VIPergic SCN neurons induces long-photoperiod-like free-running periods in mice housed in a short photoperiod both in locomotor behaviour and in the SCN itself measured ex vivo.

We also measured the effect of stimulation in vivo on phase angle of entrainment of the locomotor rhythm using a linear model to identify the mean activity peak time ("acrophase") in DD. To account for potential activity artifacts from untethering and cage transfer into DD (Figure S4), we measured the phase angle using the full DD record as well as with the first 24 h excluded. When

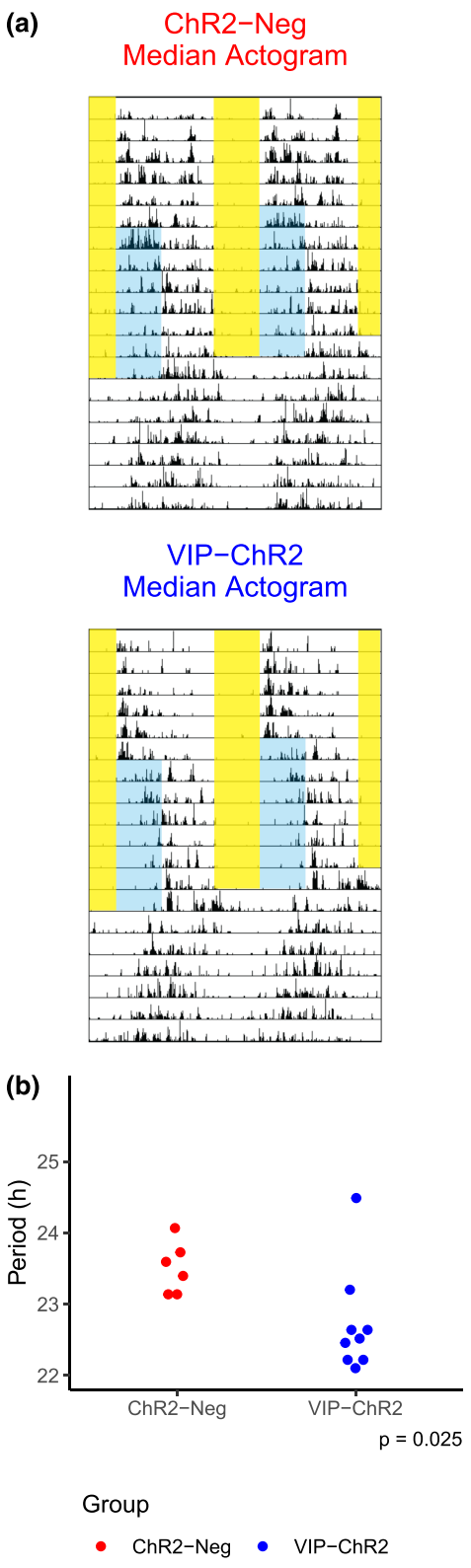

FIGURE 3 Optogenetic stimulation of VIPergic neurons influences locomotor behaviour free-running period. (a) Median actograms for ChR2-neg (top) and VIP-ChR2 (bottom) mice. Yellow shading indicates light exposure, blue shading indicates blue light stimulation of the SCN (see also Figure S1). (b) Free-running period in each group as measured by LSP on cycles 2–7 of DD. The indicated *p* value is the result of a Kruskal–Wallis test

calculated excluding the first 24 h of DD, the mean phase was ZT 0.04 (circular SD: 1.09 h) in the VIP-ChR2 group and ZT 21.13 (circular SD: 0.78 h) in the ChR2-Neg group ($p = 0.186$, circular ANOVA; Figure S5A), while phase estimates based on all 7 days of DD showed a large variance (Figure S5B). Differences in free-running period between the two groups were similar whether calculated using all 7 days of DD (Figure 3b) or excluding the first 24 h (Figure S5C).

Overall, our results elucidate a role for VIPergic neurons in initiating the sustained reconfiguration of the SCN clock network in response to changes in photoperiod. Targeted activation of SCN VIPergic neurons invoked persistent changes in SCN network configuration and function that constitute encoding of photoperiod as measured in the isolated ex vivo SCN. Indeed, we found that optogenetic stimulation in the hours following lights-off in short, winter-like photoperiods induced changes in the SCN network similar to a true lengthening of the light cycle—re-aligning the phase of SCN molecular rhythms, increasing the phase dispersion of molecular rhythms across the SCN, and shortening the free-running period of the SCN clock (Buijink et al., 2016; Ciarleglio et al., 2011; Inagaki et al., 2007; VanderLeest et al., 2007).

Because our mice were tethered with an optogenetic fibre throughout behaviour measurement, we used passive infrared detection (PID) to avoid fibre optic tangling with a cross-cage running wheel axle. The lower signal-to-noise ratio of the PID limited high-confidence manual scoring of activity duration (alpha, Figure S6). In the future, it may be possible to use axle-free running wheels with higher signal-to-noise ratio to determine the alpha after-effects following extended VIPergic SCN neuron activation.

Some optogenetic studies use enucleated mice to avoid retinal activation from fibre optic light leak (Mazuski et al., 2018). Our experiment, which required light stimulation in addition to optogenetic stimulation, precluded enucleation. We used cladded fibre optic tethers, but fibre junctions at the base of the fibre optic implant and between the implant and the tether allow some light leak. We controlled for this issue by stimulating both our experimental (VIP-ChR2) and control (ChR2-Neg) mice identically, so that any effects of retinal activation on circadian behaviour would be visible in the control group. In fact, negative masking (the phenomenon in which light exposure acutely suppresses locomotor behaviour unrelated to its timing by the circadian clock) may have occurred in some control animals during the stimulation window (Figure 3a, top; Figure S4). Consistent with the independence of masking from the circadian system, however, any effects disappear in DD in all but one control mouse (OC012, Figure S4). In experimental mice (Figure 3a, bottom), the effect on activity during the stimulation window appears stronger and persists into DD in many of the mice. The groups therefore responded differently to the treatment despite identical surgery and stimulation procedures as shown by their differences in phase following treatment in vivo (Figure S5A) and ex vivo (Figure 2b).

VIPergic neurons in the SCN have numerous roles. These neurons regulate the timing of night-time sleep in mice (Collins et al., 2020) and provide GABAergic signalling to the paraventricular nucleus (PVN) and subparaventricular zone (SPZ) that acts as a first step in the relay of circadian information in the SCN to the rest of the body (Paul et al., 2020; Todd et al., 2018). Loss of the molecular clock within VIPergic neurons affects the presentation of the locomotor behaviour rhythm, but ablation of the VIPergic neurons themselves renders animals arrhythmic (Todd et al., 2020). VIPergic neurons also play a role in the response to photoperiodic light input. Knockout of VIP disrupts circadian responses to long photoperiod, including the persistent compression of locomotor activity duration and the broadening of the SCN electrical activity waveform (Lucassen et al., 2012). As such, VIP is thought to be necessary for the encoding of photoperiod in the SCN. Here, we have shown that daily optogenetic stimulation of VIPergic neurons timed to mimic long photoperiods brings about the persistent increase in SCN network phase dispersion that underlies the broadening of the SCN electrical activity waveform and the compression of behavioural activity duration. The temporal precision of our stimulation demonstrates a specific role for VIPergic neurons in establishing the SCN network representation of photoperiod beyond previous experiments that have focused on the presence or absence of VIP itself.

Activation of VIPergic neurons was sufficient to establish additional persistent after-effects of long photoperiods in the SCN network, including a shortening of free-running period and altered phase alignment to dusk. Our lab and others have found that long and short photoperiods of 24 h T cycles have corresponding period after-effects in vivo and ex vivo, though the long-short difference is often small ex vivo (Evans et al., 2013; Green et al., 2015; Tackenberg et al., 2020). Our results here, however, show a sizable decrease in period length for the VIP-ChR2 group (Figure 2a). The larger effect size suggests that extended stimulation of the VIPergic neurons may be a powerful influence on the subsequent free-running period of the SCN network, notably one that is more fully maintained from intact brain into slice culture. The shortened free-running period may itself be a consequence of the increased phase dispersion in the SCN (Beersma et al., 2017; Buijink et al., 2016).

Interestingly, VIP also appears to play a role in returning the SCN network to baseline from reconfiguration from photoperiod (Evans et al., 2013). Taken together, our results and those of others indicate that VIP and VIPergic neuron activity are necessary and sufficient for the encoding and storage of photoperiodic information in the SCN network.

By demonstrating the sufficiency of VIPergic neurons in the induction of circadian photoperiodic encoding, we further defined the importance of this neuronal subpopulation in transmitting photic signals from the retina to shape the SCN clock network, and downstream effects of seasonal photoperiod throughout the body.

2 | METHODS

2.1 | Resource availability

2.1.1 | Lead contact

Further information and requests for resources and reagents should be directed to, and will be fulfilled by, the lead contact, Douglas G. McMahon (douglas.g.mcmahon@vanderbilt.edu).

2.1.2 | Materials availability

This study did not generate new unique reagents.

2.1.3 | Data and code availability

The code generated during this study is available at FigShare: https://doi.org/10.6084/m9.figshare.13519043

2.2 | Experimental model and subject details

2.2.1 | Mouse lines

For in vivo experiments, 5 *Vip::Cre*$^{+/-}$*Per2::Luciferase*$^{+/-}$ (4 male, 1 female) and 1 *Vip::Cre*$^{+/-}$ (male) mice were used as controls (ChR2-Neg). Nine *Vip::Cre*$^{+/-}$*floxed-ChR2*$^{+/-}$ (7 male, 2 female) were used as the experimental group (VIP-ChR2).

For ex vivo experiments, 8 *Vip::Cre*$^{\pm}$*Per2::Luciferase*$^{+/-}$ (5 male, 3 female) mice were used as controls (ChR2-Neg). Eight *Vip::Cre*$^{+/-}$*floxed-ChR2*$^{+/-}$*Per2::Luciferase*$^{+/-}$ (4 male, 4 female) mice were used as the experimental group (VIP-ChR2).

2.3 | Method details

All procedures involving mice were performed in accordance with Vanderbilt University Institution of Animal Care and Use committee regulations.

2.3.1 | Fibre optic implant surgery

Fibre optic implant surgery procedure and components are described in detail in Jones et al. (2021). We anesthetized mice with 3% isoflurane and provided ketoprofen for pre- and post-operative analgesia. After isoflurane induction, we secured the head of the mouse in a streotax and provided lubricating eye drops. We applied iodine-based antiseptic to the shaved scalp and made an incision in the skin. We applied 2% hydrogen peroxide to clean the skull of connective tissue and dried the surface with a sterile cotton swab. After levelling the skull, we used a mounted drill to make a small craniotomy at Bregma and scoured the skull surface with forceps. We lowered a 5-mm fibre optic implant into the craniotomy and stopped any bleeding that results with ophthalmic absorbent strips. We then applied Metabond to the scoured skull surface surrounding the fibre optic implant post and let it cure for 5 min, followed by a small but secure dental cement cap that was allowed to cure for 10 additional minutes. We secured the skin to the dental cement cap using sterile veterinary surgical adhesive and coated the edges of the skin with iodine-based antiseptic.

2.3.2 | Ex vivo procedure

After at least 1 week of recovery from surgery in 12:12 LD, we moved the mice to the stimulation light/dark box, still in standard shoebox cages (no running wheel, no PID attachment) so that no acclimation was necessary before tethering. We immediately attached these mice to the fibre optic tethers and stimulation began at the time of lights-off that evening. After 7 days of daily stimulation, we extracted and cultured 300-μm slices of SCN for PER2 luminescence recording.

We made SCN slices 2–4 h before the timing of lights-off. Our slicing media was composed of 100 ml of 10× HBSS, 10 ml of 10,000 U/mL PenStrep, 5 ml of 7.5% sodium bicarbonate, and 2.38 g of HEPES per 1000 ml sterile water. The slicing solution was chilled and kept cold in an ice bath during slicing. Our slice culture media was composed of DMEM with L-glutamine (Sigma D2902), 4.7 ml of 7.5% sodium bicarbonate, 2.38 g HEPES, 2.5 ml of 10,000 U/ml PenStrep, and 3.5-g D-glucose per 1000-ml sterile water. For 6 ml of culture

media, we added 6 μl of 0.1-M luciferin and 120 μl of 50X B-27. We cultured the slices in a six-well plate with 1.2 ml of culture media in each well, with a sterile culture membrane on top. We sealed the plates with PCR plate sealing film and imaged the slices using an inverted microscope with an intensified CCD camera attached. We imaged each slice once per 10 min, using an aggregation time of 2 min, and continued recordings for 6 days.

2.3.3 | In vivo procedure

We used a separate cohort of mice undergoing the same surgical and recovery procedures for our in vivo studies. After recovery in 12:12 LD, we moved animals to 8:16 LD (short photoperiod) in cages with passive infrared detectors (PIDs) attached. There were no running wheels in the recovery or experimental cages. We housed mice for 2 days without attachment to the fibre optic tethers to acclimate to the PID cages. On the second full day, we attached mice to the fibre optic tether, and the following 5 days were designated as the "Baseline" portion of the experiment. On the sixth day, the LEDs began turning on for 8 h each day at 10 Hz, starting at lights-off. To avoid any effect of a dark pulse between the termination of light and the onset of stimulation, we set the stimulation to overlap the light cycle by $\sim$ 3 min. After seven full days of daily stimulation, we moved the cages of the mice into a nearby light/dark box for the constant darkness (DD) portion of the experiment. Cage transfers were done in dim red light. After seven full days in DD, we ended the experiment.

Two mice (one each from ChR2-Neg and VIP-ChR2) were re-run through the in vivo procedure due to an LED failure and a PID failure, respectively. Neither of these mice were transferred to DD, but rather remained in the stimulation light/dark box for the following run-through of the protocol. Neither mouse received fibre optic stimulation during their initial, failed trial, but did receive extra days of 8:16 photoperiod as a result.

2.4 | Quantification and statistical analysis

2.4.1 | Ex vivo analyses

Each SCN slice image corresponded to $\sim$6 cycles of PER2::LUC bioluminescence with a resolution of six frames per hour. We processed each image in ImageJ first using a two-frame minimization to remove CCD noise (reducing frame rate to three frames per hour) followed by an overlay of a grid of 10,404–10 $\times$ 10 μm ROIs. We exported the "stack grid" of the luminescence profiles of each ROI into R for further analysis. We limited our analyses to ROIs within the top 20th percentile of overall luminescence intensity in each slice, thus focusing the analyses on the SCN tissue. For the PER2::LUC trace in each ROI, we smoothed using a Savitzky–Golay filter (order of 2, span of 51) and baseline subtracted using a more heavily smoothed Savitzky–Golay filtering of the trace (order of 5, span of half the number of frames). For each baseline-subtracted, smoothed trace, we identified up to six peaks (at least 18 h apart).

To eliminate artificial or partial first peaks, we established a starting cut-off at 18 h post-culture (Figure S5A). From that starting cut-off, we used a sliding 24-h window to assign peak numbers to each detected peak regardless of the order identified (this prevents a missed peak from altering all subsequent peak times, Figure S5B). For example, if ROI A identified peaks at 24, 48, and 72 h and ROI B identified peaks at 24 and 72 h, this step will appropriately designate ROI A's peaks as Peak 1, Peak 2, and Peak 3 and ROI B's peaks as Peak 1 and Peak 3.

Using this processing, we calculated the mean peak time of each overall peak and calculated the phase of each ROI relative to the mean timing of that peak for that slice. For each peak in each slice, we calculated the median absolute deviation of peak times and performed an ordinary two-way ANOVA to measure the main effect of peak number and group.

With the same starting cut-off of 18 h, we measured free-running period of the PER2::LUC rhythm using the Lomb–Scargle periodogram. We compared the groups using a Kruskal–Wallis test on ranks.

We measured phase as the mean time of the first peak for each slice. Like our in vivo analysis, we compared the phase of the two groups using a circular ANOVA, while calculating the circular mean and standard deviation of each group.

2.4.2 | In vivo analyses

We generated median actograms using ClockLab Analysis (Actimetrics).

We estimated the acrophase for each mouse in each cycle following the final stimulation offset. In R, we fit a linear regression of the acrophase for cycles 1–7 or cycles 2–7 to retroject the acrophase of the final day before DD. We analysed phase differences between the two groups using a circular ANOVA with the circular package. Using the same package, we calculated circular means and standard deviation.

We measured free-running period using the Lomb–Scargle periodogram on the counts (1-min resolution) for cycles 1–7 (Figure 3b) or cycles 2–7 (Figure S5C) from each actogram exported to R. We analysed the free-running period using a Kruskal–Wallis test on ranks.

ACKNOWLEDGEMENTS

We would like to thank Jeff Jones and Elliot Outland for helpful discussions. This work was supported by NIH R01 GM117650 to D.G.M. and NIH R35 GM124685 to J.J.H.

CONFLICT OF INTEREST

The authors declare no conflicts of interest.

AUTHOR CONTRIBUTIONS

M.C.T. and D.G.M. designed the experiments. M.C.T. performed the experiments. M.C.T. and J.J.H. analysed the data. M.C.T., J.J.H., and D.G.M. wrote the paper.

PEER REVIEW

The peer review history for this article is available at https://publons.com/publon/10.1111/ejn.15442.

DATA AVAILABILITY STATEMENT

The data that support the findings of this study are available from the corresponding author upon reasonable request.

ORCID

Michael C. Tackenberg https://orcid.org/0000-0003-0220-865X

Jacob J. Hughey https://orcid.org/0000-0002-1558-6089

REFERENCES

Beersma, D. G. M., Gargar, K. A., & Daan, S. (2017). Plasticity in the period of the circadian pacemaker induced by phase dispersion of its constituent cellular clocks. *Journal of Biological Rhythms*, *32*, 237–245. https://doi.org/10.1177/0748730417706581

Buijink, M. R., Almog, A., Wit, C. B., Roethler, O., Olde Engberink, A. H. O., Meijer, J. H., Garlaschelli, D., Rohling, J. H. T., & Michel, S. (2016). Evidence for weakened intercellular coupling in the mammalian circadian clock under long photoperiod. *PLoS ONE*, *11*, e0168954. https://doi.org/10.1371/journal.pone.0168954

Ciarleglio, C. M., Axley, J. C., Strauss, B. R., Gamble, K. L., & McMahon, D. G. (2011). Perinatal photoperiod imprints the circadian clock. *Nature Neuroscience*, *14*, 25–27. https://doi.org/10.1038/nn.2699

Collins, B., Pierre-Ferrer, S., Muheim, C., Lukacsovich, D., Cai, Y., Spinnler, A., Herrera, C. G., Wen, S., Winterer, J., Belle, M. D. C., Piggins, H. D., Hastings, M., Loudon, A., Yan, J., Földy, C., Adamantidis, A., & Brown, S. A. (2020). Circadian VIPergic neurons of the suprachiasmatic nuclei sculpt the sleep-wake cycle. *Neuron*, *108*, 486–499.e5. https://doi.org/10.1016/j.neuron.2020.08.001

Evans, J. A., Leise, T. L., Castanon-Cervantes, O., & Davidson, A. J. (2013). Dynamic interactions mediated by nonredundant signaling mechanisms couple circadian clock neurons. *Neuron*, *80*, 973–983. https://doi.org/10.1016/j.neuron.2013.08.022

Green, N. H., Jackson, C. R., Iwamoto, H., Tackenberg, M. C., & McMahon, D. G. (2015). Photoperiod programs dorsal raphe serotonergic neurons and affective behaviors. *Current Biology*, *25*, 1389–1394. https://doi.org/10.1016/j.cub.2015.03.050

Inagaki, N., Honma, S., Ono, D., Tanahashi, Y., & Honma, K.-I. (2007). Separate oscillating cell groups in mouse suprachiasmatic nucleus couple photoperiodically to the onset and end of daily activity. *Proceedings of the National Academy of Sciences of the United States of America*, *104*, 7664–7669. https://doi.org/10.1073/pnas.0607713104

Jones, J. R., Simon, T., Lones, L., & Herzog, E. D. (2018). SCN VIP neurons are essential for Normal light-mediated resetting of the circadian system. *The Journal of Neuroscience*, *38*, 7986–7995. https://doi.org/10.1523/JNEUROSCI.1322-18.2018

Jones, J. R., Tackenberg, M. C., & McMahon, D. G. (2021). Optogenetic methods for the study of circadian rhythms. In S. A. Brown (Ed.), *Circadian clocks: Methods and protocols* (pp. 325–336). New York, NY: Springer US. https://doi.org/10.1007/978-1-0716-0381-9_24

Lucassen, E. A., van Diepen, H. C., Houben, T., Michel, S., Colwell, C. S., & Meijer, J. H. (2012). Role of vasoactive intestinal peptide in seasonal encoding by the suprachiasmatic nucleus clock. *The European Journal of Neuroscience*, *35*, 1466–1474. https://doi.org/10.1111/j.1460-9568.2012.08054.x

Mazuski, C., Abel, J. H., Chen, S. P., Hermanstyne, T. O., Jones, J. R., Simon, T., Doyle, F. J. 3rd, & Herzog, E. D. (2018). Entrainment of circadian rhythms depends on firing rates and neuropeptide release of VIP SCN neurons. *Neuron*, *99*, 555–563.e5.

Myung, J., Hong, S., DeWoskin, D., De Schutter, E., Forger, D. B., & Takumi, T. (2015). GABA-mediated repulsive coupling between circadian clock neurons in the SCN encodes seasonal time. *Proceedings of the National Academy of Sciences of the United States of America*, *112*, E3920–E3929. https://doi.org/10.1073/pnas.1421200112

Paul, S., Hanna, L., Harding, C., Hayter, E. A., Walmsley, L., Bechtold, D. A., & Brown, T. M. (2020). Output from VIP cells of the mammalian central clock regulates daily physiological rhythms. *Nature Communications*, *11*, 1453. https://doi.org/10.1038/s41467-020-15277-x

Pittendrigh, C. S., & Daan, S. (1976). A functional analysis of circadian pacemakers in nocturnal rodents (I). *Journal of Comparative Physiology*, *106*, 223–252. https://doi.org/10.1007/BF01417856

Shan, Y., Abel, J. H., Li, Y., Izumo, M., Cox, K. H., Jeong, B., Yoo, S.-H., Olson, D. P., Doyle, F. J. 3rd, & Takahashi, J. S. (2020). Dual-color single-cell imaging of the suprachiasmatic nucleus reveals a circadian role in network synchrony. *Neuron*, *108*, 164–179.e7. https://doi.org/10.1016/j.neuron.2020.07.012

Tackenberg, M. C., & Hughey, J. J. (2021). The risks of using the chi-square periodogram to estimate the period of biological

rhythms. *PLoS Computational Biology*, *17*, e1008567. https://doi.org/10.1371/journal.pcbi.1008567

Tackenberg, M. C., Hughey, J. J., & McMahon, D. G. (2020). Distinct components of photoperiodic light are differentially encoded by the mammalian circadian clock. *Journal of Biological Rhythms*, *35*, 353–367. https://doi.org/10.1177/0748730420929217

Tackenberg, M. C., & McMahon, D. G. (2018). Photoperiodic programming of the SCN and its role in photoperiodic output. *Neural Plasticity*, *2018*, 8217345. https://doi.org/10.1155/2018/8217345

Todd, W. D., Fenselau, H., Wang, J. L., Zhang, R., Machado, N. L., Venner, A., Broadhurst, R. Y., Kaur, S., Lynagh, T., Olson, D. P., Lowell, B. B., Fuller, P. M., & Saper, C. B. (2018). A hypothalamic circuit for the circadian control of aggression. *Nature Neuroscience*, *21*, 717–724. https://doi.org/10.1038/s41593-018-0126-0

Todd, W. D., Venner, A., Anaclet, C., Broadhurst, R. Y., De Luca, R., Bandaru, S. S., Issokson, L., Hablitz, L. M., Cravetchi, O., Arrigoni, E., Campbell, J. N., Allen, C. N., Olson, D. P., & Fuller, P. M. (2020). Suprachiasmatic VIP neurons are required for normal circadian rhythmicity and comprised of molecularly distinct subpopulations. *Nature Communications*, *11*, 4410. https://doi.org/10.1038/s41467-020-17197-2

VanderLeest, H. T., Houben, T., Michel, S., Deboer, T., Albus, H., Vansteensel, M. J., Block, G. D., & Meijer, J. H. (2007). Seasonal encoding by the circadian pacemaker of the SCN. *Current Biology*, *17*, 468–473. https://doi.org/10.1016/j.cub.2007.01.048

SUPPORTING INFORMATION

Additional supporting information may be found in the online version of the article at the publisher's website.

How to cite this article: Tackenberg, M. C., Hughey, J. J., & McMahon, D. G. (2021). Optogenetic stimulation of VIPergic SCN neurons induces photoperiodic-like changes in the mammalian circadian clock. *European Journal of Neuroscience*, *54*(9), 7063–7071. https://doi.org/10.1111/ejn.15442